ERSD 2018

KỶ YẾU

HỘI NGHỊ TOÀN QUỐC
KHOA HỌC TRÁI ĐẤT VÀ TÀI NGUYÊN VỚI PHÁT TRIỂN BỀN VỮNG

Hà Nội, 07 - 12 - 2018

ĐỊA CHẤT VÀ TÀI NGUYÊN ĐỊA CHẤT

Nhà xuất bản giao thông vận tải

MỤC LỤC

TIỂU BAN
ĐỊA CHẤT VÀ TÀI NGUYÊN ĐỊA CHẤT

HỘI NGHỊ TOÀN QUỐC KHOA HỌC TRÁI ĐẤT
VÀ TÀI NGUYÊN VỚI PHÁT TRIỂN BỀN VỮNG (ERSD 2018)

Apply electromagnetic approach to study saltwater intrusion in Crau coastal aquifers, France

Nguyễn Bách Thảo[1,2*]
[1] *Faculty of Geosciences and Geo-engineering, Hanoi University of Mining and Geology*
[2] *Centre for Excellence in Analysis and Experiment (CEAE) , Hanoi University of Mining and Geology*

ABSTRACT

Coastal aquifers constitute an important high-quality freshwater resource exploited for agriculture, industry and human consumption. An increase in salinity occurs close to the sea, highlighting the need to investigate the water balance and groundwater behavior. Normally, this task could be solved by using monitoring and groundwater modeling. The main difficulty is to parameterize and calibrate/validate the variable-density modeling. This requires adequate information on aquifer parameters and concentration distribution in groundwater. To solve this problem, we propose to use geophysical investigations to describe and image the transition zone of the freshwater/saltwater. Such investigations can help to setup and validate the variable-density flow models. Electromagnetic method has been used to determine saltwater intrusion in groundwater in this aquifer by using EM34 equipment (Geonics Ltd). This method has been applied succesful in Crau aquifer, southeastern France, where hydrological characteristics are similar to coastal aquifers in Vietnam.
Từ khóa: Electromagnetic, EM34, Saltwater intrusion, Coastal aquifer

1. Introduction

One of the most popular geophysical methods currently used to provide information about the spatial variation of soil properties is electromagnetic (EM) induction (Triantafilis and Monteiro Santos, 2013). EM methods were originally developed for mine exploration and have been widely used over the last decades for engineering purposes (McNeill, 1980) and for groundwater investigations (Fitterman and Deszcz-Pan, 2004) and its cost effective, reliable. These techniques have been described in geophysical handbooks and scientific papers (McNeill, 1980, Stewart, 1982, Stewart and Gay, 1986, Borne, 1990, Triantafilis et al., 2003, Santos, 2004). Then, despite the qualitative nature of the provided information, this method is widely applied for hydrogeological and environmental investigations. Many applications of EM surveys have been applied for resources management in coastal aquifer (Stewart, 1982, Goldman et al., 1991, Frohlich et al., 1994)

With the development of the EM31 and the EM34-3 (Geonics Ltd) it is possible to map terrain conductivity virtually as fast as the operators can walk and at low costs. The interpretation of EM data by using some modeling programs is qualitative even their inversion can be done for layered models.

2. Methodology

2.1. Principle of operation

In this study, we employed an EM34-3 of Geonics (Figure 1) to directly measure bulk conductivity. This equipment consists of two coils. One is the transmitter which is energized with an alternating current at a specific frequency and other is the receiver. The transmitter creates a magnetic field in the subsurface while the receiver detects and records the magnetic field. These two coils can be operated with different spacing of 10, 20 and 40m to vary the depth of exploration. Changing the orientation of transmitter/receiver loops from the vertical to the horizontal (Figure 2) also varies the depth of exploration by increasing the 70% response from 0.75 to 1.5 time the intercoil spacing (McNeill, 1980). The use of different intercoil spacing with different frequencies (6400, 1600 and 400 Hz) and different loops orientation vertical and horizontal allows to construct an image of subsurface electrical conductivity distribution from 7.5 meters to a maximum of 60 meters (Santos, 2004).

[*] *Tác giả liên hệ*
Email: nguyenbachthao@humg.edu.vn

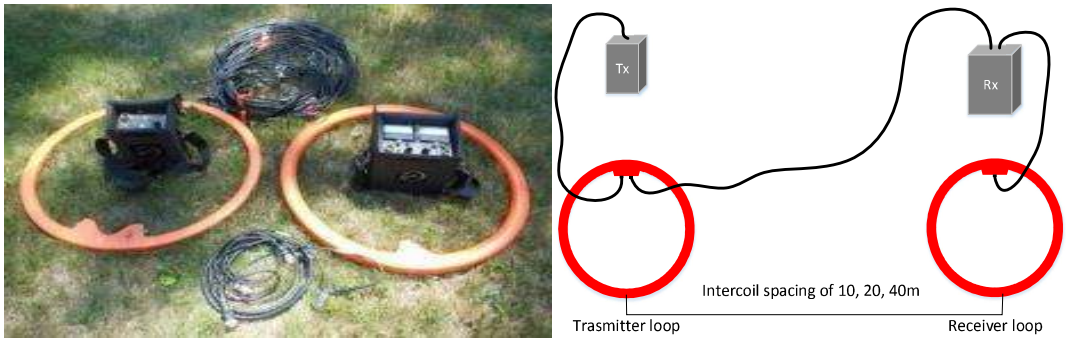

Figure 1. Geonics Electromagetic EM34-3 instrument applied in study area

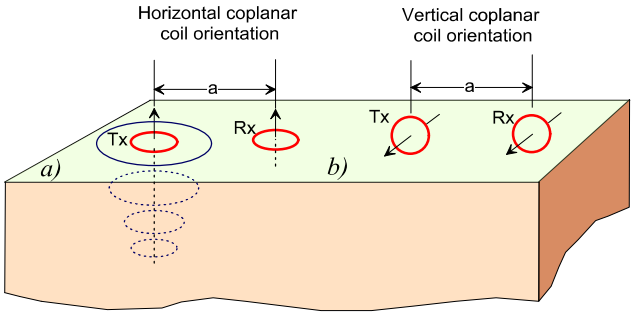

Figure 2. Relative response versus depth for (a) vertical dipoles and (b) horizontal dipoles

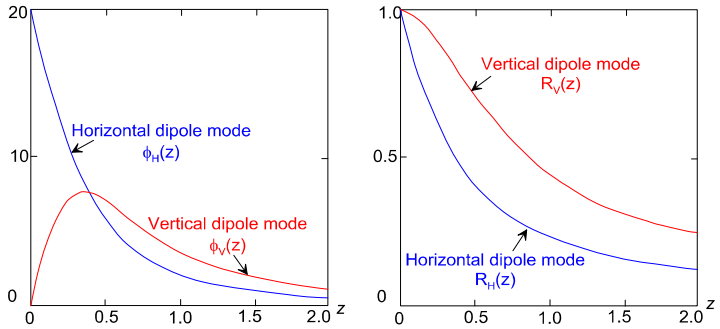

Figure 3. Comparison of relative responses for vertical and horizontal dipole modes. Note x axis = depth/intercoil spacing. (reproduced from McNeill, 1986)

Consider to Figure 3, in which a transmitter coil *Tx* energized with an alternating current at an audio frequency, is placed on the earth and a receiver coil *Rx* is located a short distance *s* away.

The time-varying magnetic field arising from the alternating current in the transmitter coil induces very small currents in the earth which generates a secondary magnetic field H_s which is sensed, together with the primary field, H_p, by the receiver coil. In general, this secondary magnetic field is a complicated function of the intercoil spacing *s*, the operating frequency, *f*, and the ground conductivity σ. Under certain constraints, technically defined as "operation at low values of induction number", the secondary magnetic field is a very simple function of these variables. These constraints are incorporated in the design of the EM31 and EM34-3 whence the secondary magnetic field is shown to be

$$\frac{H_s}{H_p} \cong \frac{i\omega\mu_0\sigma s^2}{4}$$

Where:
H_s: secondary magnetic field at the receiver coil
H_p: primary magnetic field at the receiver coil
$\omega = 2\pi\phi$

f = frequency (Hz)

μ_o = permeability of free space

σ = groundwater conductivity (mho/m)

s = intercoil spacing (m), $i = \sqrt{-1}$

The ratio of the secondary to the primary magnetic field is now linearly proportional to the terrain conductivity, a fact which makes it possible to construct a direct-reading, linear terrain conductivity meter by simply measuring this ratio. Given H_s/H_p the apparent conductivity indicated by the instrument is defined from equation as below:

$$\sigma_s = \frac{4}{\omega \mu_0 s^2}\left(\frac{H_s}{H_p}\right)$$

2.2. Interpretation

Usually the interpretation of the EM34-3 data is qualitative. One-dimensional modeling or inversion is possible (Santos et al., 2002).

A mesh of prismatic blocks centered at each measurement point, as is usual in three-dimensional modeling, make up the earth model. The program inverts all the data set jointly, using the cumulative response (McNeill, 1980) approach at each site of the grid of measurements to calculate the forward response and derivatives. Spatial smoothness constraints are introduced during the inversion procedure in order to construct a conductivity model, which represents the main features contained in the data. Two inversion algorithms are given by Sasaki. The least square solution of such a non-linear smoothing problem is (Sasaki, 1989):

$$\left[\left(J^T J+\lambda C^T C\right)\right]\delta p = J^T b$$

And in the second algorithm (Sasaki, 2001), the equation is :

$$\left[\left(J^T J+\lambda C^T C\right)\right]\delta p = J^T b+\lambda C^T C\left(p-p_o\right)$$

Here δp is the vector containing the corrections applicable to the model parameters, p_o is a reference model, b is the vector of the differences between the logarithm of the observed and the calculated σ_a, J is the Jacobian matrix, the superscript T is the transpose operation and λ is a Lagrange multiplier that controls the amplitude of the parameter corrections and the elements of the matrix C are the coefficients of the values of the roughness in each parameter which is defined in term (Sasaki, 1989). Although the final result obtained applying such a method is only a rough approach of a three-dimensional model and, for this reason it is designated as quasi-three-dimensional model, it can be very useful in the global interpretation of surveys.

Therefore, we have some difference methods of interpretation:

i) Direct interpretation using multiple EM readings at selected locations apply (empirical) formulae and using EMIX34 computer software;

ii) Analysis of relative readings (shows area of saline water and fresher water);

iii) Correlation of results with other more direct techniques:

– Salinity profiles from boreholes on same island;

– Salinity profiles from islands with similar geology;

– Electrical resistivity soundings.

3. Research area

The Crau coastal plain is a paleo-delta of the Durance River, located in the Southeastern of France, East of the present delta of the Rhône River, which is also known under the name of Camargue. The Crau aquifer delimited by Alpilles mountains in the North and by the Mediterranean sea in the South, forming a triangular area of about 600 km^2 between Arles, Salon-de-Provence and Fos. The aquifer is mostly recharged by direct infiltration of rainfall, irrigation practices and lateral groundwater flows. The irrigation of about 15,000 ha of meadow is done using water from the Durance supplied by a dense network of channels (Olioso et al., 2013). Groundwater naturally discharges into the marshes and the Rhône River. Intensive withdrawal occurs from pumping wells. The Crau aquifer is the main resource of domestic water for more than 300,000 inhabitants. It is important to notice that there is no natural river over the Crau plain and that all the surface water transfers occur through artificial canals.

In this study, our approach was applied on an area of about 140 km^2, is situated in downstream part of the Crau coastal plain, what is now called “Study area” where located the salt/fresh water interface shown in Figure 4.

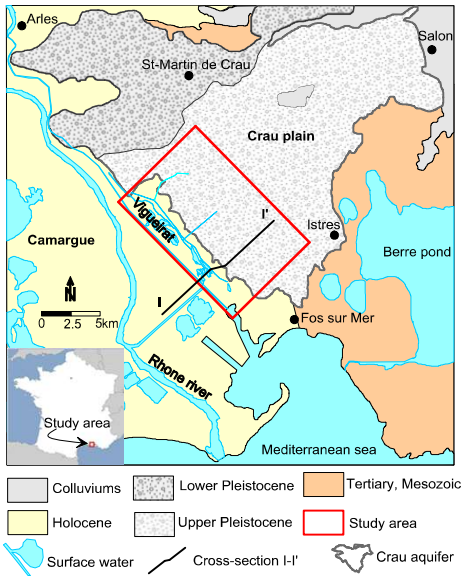

Figure 4. Location of Crau coastal plain and the study area.

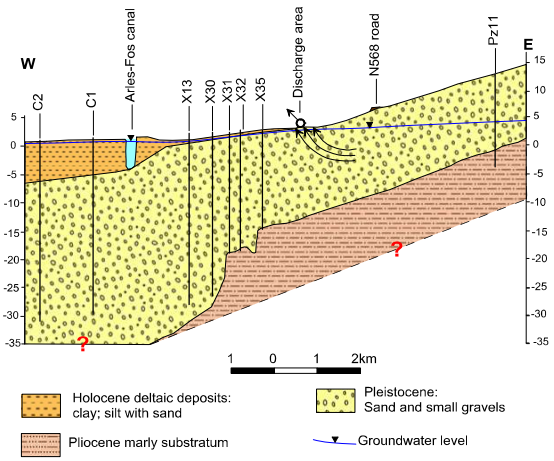

*Figure 5. Schematic of hydrogeological cross section **I-I'** (BRGM, edited)*

The study area was considered a suitable case of study area because: (i) it is an important aquifer in the South of France, highly vulnerable to salinization due to its coarse nature; (ii) groundwater salinity problems have occurred due to a great number of groundwater extraction wells for irrigation and the changes in the water management; (iii) the groundwater abstraction for domestic/industrial use caused significant variation of water heads; (iv) a dataset over a 20 year period is available for the site.

The Crau aquifer is globally unconfined, but becomes semi-confined to confined in the marsh area of Vigueirat and Landre ponds (Figure 5), due to the presence of semi-pervious material (Rhone River sediment and lacustrine deposits). This material has low hydraulic conductivity (between 3.7x10-5 and 8.7x10-3 m/s) and its thickness in the study area varies from 0m at the limit of Crau aquifer to more 7m near Arles-Fos canal. The specific yield of aquifer obtained from pumping tests is in the range of 0.01 to 0.18 attesting the unconfined to semi-confined (leaky) behavior of aquifer.

4. Results and discussion

Two campaigns of EM surveys have been conducted (Figure 6) in marsh area around the saltwater front which was defined by electrical conductivity measurements .

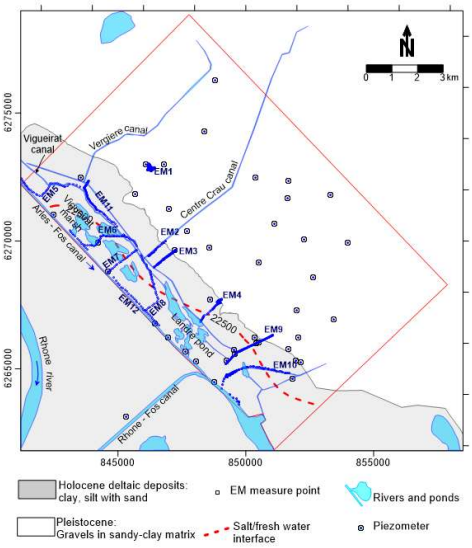

Figure 6. Position of electromagnetic (EM34) measurement points

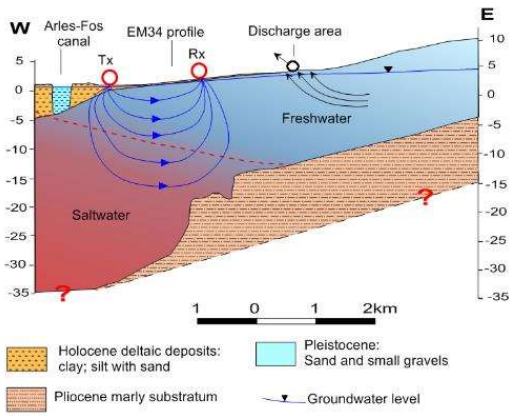

Figure 7. Principle of EM34 profile with regard to interface between fresh and salt water of cross section I-I'.

Principle EM profile with regard to saltwater front is shown in Figure 7. The first campaign have been carried out in four sectors northeastern side of the canal Colmatage (sectors 1-4) and the second campaign in eight sectors on the other side of canal (sectors 5-12). The transmitter-receiver separation was 10m (EM34-10) and 20m (EM34-20) with both vertical dipole (VD) and horizontal dipole (HD). Distance between sectors varies from about 600 m to 11 km. 480 points where measured with EM34-10, 853 points with EM34-20 and 30 points with EM34-40 (Table 1). The topography in marsh area is flat at a level between 0-1 m.asl in the marsh zone and 2-3 m.asl in the sector 1-4. In several sectors, some measurements with an intercoil separation of 40m (EM34-40) have been added in order to image the apparent electrical conductivity distribution at the difference depths. These surveys have covered distances of more than 30km (Figure 6, Table 1).

Table 1. EM34 profiles in research area

Sector	Location	Distance	Measurements (point)	
		(m)	*EM34-10*	*EM34-20*
1	Center Crau (nearby P21, P21bis)	1,600	90	73
2	Along Center Crau canal	909		22
3	Nearby X20 piezometer	1,153		32
4	Nearby X26 piezometer	1,235	29	36
5	Northern of Vigueirat	1,977	57	57
6	Center of Vigueirat, nearby XB	2,028		40
7	Center of Vigueirat, nearby X19	1,426	33	33
8	Southern of Vigueirat	2,598		121
9	Sector Pissarotte, nearby X13, X31	2,236	117	96
10	Sector Tonkin	2,599	28	83
11	Along Colmatage canal	5,849		107
12	Along canal Arles-Fos	6,800	126	153
	Total	**30,410**	**480**	**853**

Figure 8. EM34 measurement in study area

After two campaigns of EM survey, 12 profiles of EM34 have been done (Figure 6 and Table 1) in the marsh area, with 10 profiles perpendicular with salt-freshwater limit and two others along the canals. The spatial distribution of apparent soil electrical conductivity (σ_a - mS/m) of EM34-20 have been compared with a spatial distribution of electrical conductivity (EC) measurements from in pore water at 10 m depth. The small σ_a (<30 mS/m) characterize the freshwater zone in the center and northeast of Crau. In the zone along the Colmatage canal in center of marsh area, σ_a varies from 30-80 mS/m characterize a saline intrusion zone, equivalent to EC from 6000-18000 µS/cm. In the southwest area, σ_a is very high (>100 mS/m) characterize the saltwater zone.

The EM34 data have been interpreted by using the software EM4Soil - a software package which was developed to enable the inversion of electromagnetic (EM) conductivity data σ_a acquired at low induction numbers (EMTOMO, 2015). The inversion algorithm is based upon the Occam regularization method (Sasaki, 1989, Sasaki, 2001) was described and applied in several studies (Santos et al., 2010, Triantafilis and Monteiro Santos, 2013, Triantafilis et al., 2013). With the inverse model, EM34 apparent

conductivity (σ_a) were inverting using a 1-D spatially constrained algorithm for quasi-3D conductivity imaging, then a map of spatial distribution of estimated electrical conductivity σ have been done would help to better understand in term of geology (structure, lithology,…) and hydrogeology (saline groundwater interface, …).

The first campaign, studying the thickness and geometry of depositional systems, using intercoil spacing of 10 and 20 m, has been applied on 4 sectors in the NE of the Colmatage canal. This sector contains freshwater and is far from salt-freshwater limit as determined by electrical conductivity measured in piezometers. The second campaign have been developed around the salt intrusion zone described by previous studies (SAFEGE, 2006). This campaign was dedicated to understand the current distribution of salt and brackish water in this aquifer.

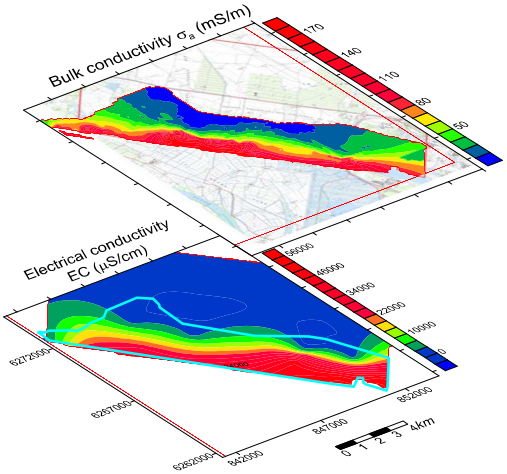

Figure 9. Spatial distribution of appaeent electrical conductivity □$_a$ (mS/m) with EM34-20m HDM (upper) and electrical conductivity ECe (□S/cm) in groundwater at -10m depth from groundwater level in piezometers (lower), red and blue colors represent the conductive and resistive layers, respectively.

Table 2. EM-34 survey measurement statistics

Sensor	Readings	Mean+-1std dev.	Std dev.	Min	Max
VDM-10m	435	77.38	64.83	7.13	201.30
HDM-10m	435	29.17	24.74	3.80	93.34
VDM-20m	774	58.99	38.30	10.50	198.07
HDM-20m	774	60.12	48.75	9.70	232.65
VDM-40m	30	62.32	13.65	49.00	112.60
HDM-40m	30	42.97	2.87	38.60	48.00

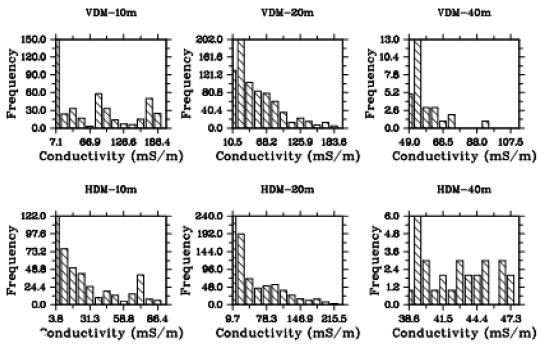

Figure 10. EM34 data statistic of all measurements .

To interpret the spatial distribution of electrical conductivity σ within these sectors, one campaign of electrical conductivity ECe profiling in boreholes has been done at the same period of geophysical campaign. Two perpendicular sectors of ECe have been investigated, one along the road N286 (Figure 11) and the other along the canal from Arles-Fos (Figure 12). On both profiles, spatial distribution of ECe is clear. Spatial maps of estimated σ from electromagnetic EM34 were compared to the spatial maps of

ECe. The spatial, vertical distribution of ECe measured in piezometers (Figure 11) shows that the saltwater comes from SW to NE. Saltwater (with ECe > 2250 mS/m) from -10 m in X4415, and from -14 m in X13 but in X33, ECe at -20 m is only 2030 mS/m. The spatial distribution map of σ (Figure 11) shows a similar pattern with higher conductivity in the SW, and decrease to the NE. High value of electrical conductivity σ > 150 mS/m is observed at about 10 m depth in X13 but disappears even at -20 m depth in X31.

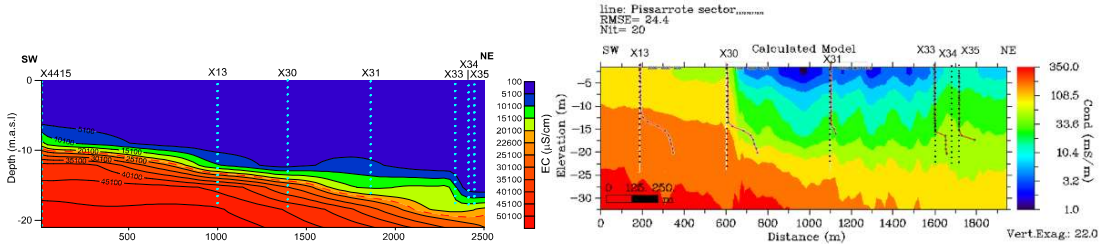

Figure 11. Spatial distribution of upper) electrical conductivity water in piezometers (ECe – µS/cm) and below) estimated electrical condutivity from EM34 apparent electrical conductivity (σ_a – mS/m) in sector EM9 (Pissarote)

It is similar for the sector along the Arles-Fos Canal. A spatial distribution of σ was obtained from the apparent survey electricity with root mean square error (RMSE) of 28.0%. The 2-D estimated σ profile shows that the higher σ are distributed in SE and decrease to NW direction. From Figure 12 the depth of saline groundwater with ECe > 2250 mS/m have been found at 14 m depth in L1 and are not present in X21 (at 18m). Comparing the pattern of two sectors, the saline groundwater zone from Figure 12 has the pattern of σ > 150 mS/m and fresh water zone with σ between 5 and 40 mS/m. From the pattern of the distribution of the estimated electrical conductivity and electrical conductivity of water in piezometers from Figure 11 and Figure 12, the inverse models compared favorably with the electrical conductivity profiles obtained from piezometer measurements. It is obvious that the distribution of σ confirms the presence of saline groundwater.

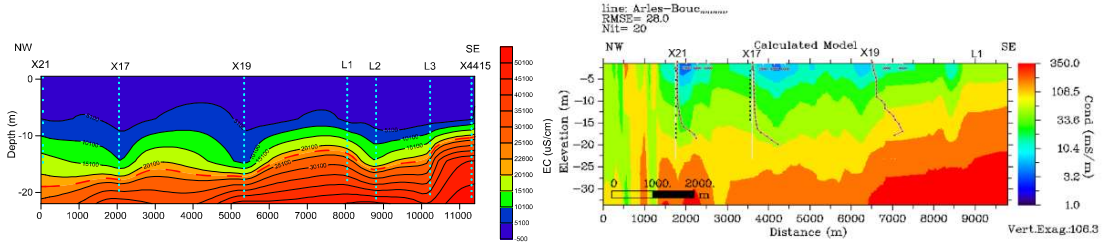

Figure 12. Spatial distribution of a. electrical conductivity water in piezometers (ECe – □S/cm) and b. estimated electrical condutivity from EM34 apparent electrical conductivity □$_a$ – mS/m) in sector EM12 along the canal from Arles-Fos.

In sector 1, the small σ (less than 2 mS/m) have been found from top to about 4 m depth. One can distinguish the water table in the aquifer (water table in Pz21 is 3.15 m). In some sectors, σ of the top soil (few meters depth) is very high (σ > 150mS/m) and compares to the values of ECe smaller than 20 mS/m (fresh water). These zones coincide with the clay layer described in piezometers XB, X19, L1. The electrical conductivity is high in some places because: 1) water table is very low about 0.3 m to 0.7 m from the surface; 2) saltwater table is shallow (less than 10 m); 3) surface water is not connected to pond or canals and 4) effect of evapo-transpiration that concentrates salt in water. In comparison, the saturated sand and gravels layer with fresh water (ECe < 200 mS/m) is characterized by σ ranging between 5 and 40 mS/m.

In sector EM12 along the Arles to Fos canal, the value of RMSE is 28% and could be due to the low resolution of σ_a along this sector. The sector is too long (>10km), and data of EM34 is discontinue in some parts because of the security regulation of Vigueirat (cows and bulls grazing).

Despite these comparisons and validations, electrical conductivity σ appears to sign the presence of saltwater and the difference of lithology. Therefore, the spatial distribution of σ from quasi 3-D imaging have been done to validate and calibrate at difference depths the saltwater model (Figure 13).

Figure 13 shows the spatial pattern of estimated electrical conductivity from EM34 data at difference depths. All distributions show a high conductivity zone in the southwestern part of the area. These

conductive zone can potentially present saltwater intrusion. Coupled with 2-D cross sections (Figure 11, Figure 12), interpretation for the different depth has been done. With the respect to soil type and conductivity, the depth of clay layer and the interface of salt-fresh water have been determined.

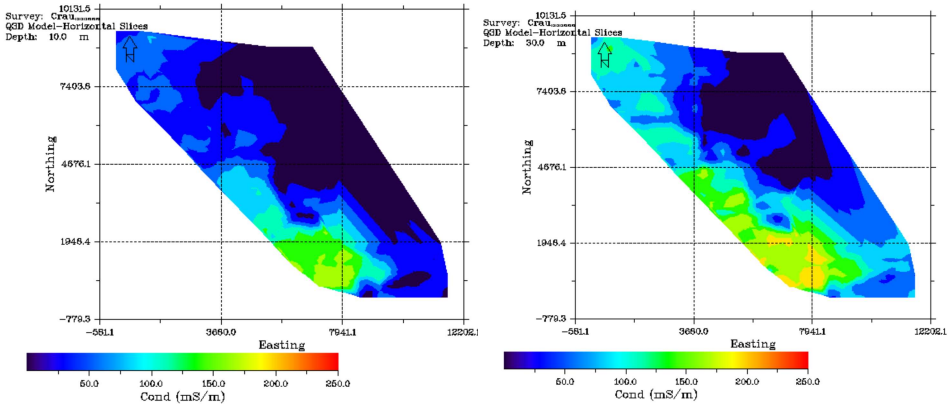

Figure 13. Spatial distribution of estimated EC (ms/m) at 10m and 30m depth from a joint inversion of EM34-10, EM34-20 and EM34-40 data using a 1-D laterally contrained algorithm for quasi-3D conductiviy imaging;

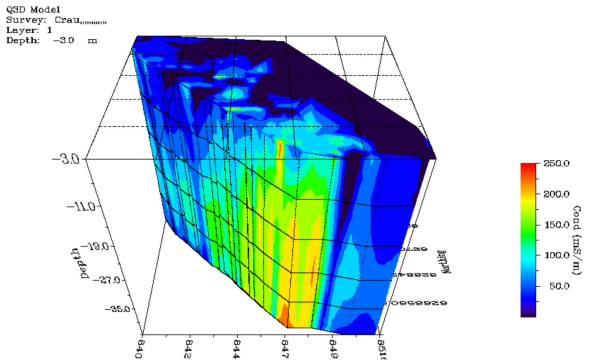

Figure 14. 3D distribution of estimated EC (σ- ms/m) from a joint inversion of EM34-10, EM34-20 and EM34-40 data using a 1-D laterally contrained algorithm for quasi-3D EC imaging

Resistivity distributions from EM and ERT methods show four different layers. i) A superficial unsaturated layer made of coarse sand and gravel (thickness of about 6 m) in the northeastern part of marsh area (center of research area) with very low $\sigma < 2$ mS/m; ii) a saturated coarse sand and gravel layer with fresh water where σ ranges from 2 to 30 mS/m; iii) a superficial fine sand and clay layer found in marsh area where σ varies from 100 to more than 300 mS/m and iv) a conductive ($\sigma > 80$mS/m) coarse sand and gravel layer saturated by brackish or saltwater observed between 3-7 and 30 m depth in sector Pissarotte and between 15-20 and 30 m depth in Vigueirat area (Figure 11 and Figure 12).

The electrical conductivity of aquifer increases with depth and towards SW due to saltwater. The most conductive area is found in sector Pissarotte (Figure 11) and in sector along the Arles-Fos canal (Figure 12) with $\sigma > 150$ mS/m at a depth less than 10 m. This characteristic is observed for all other sectors in the marsh area.

The variation of electrical conductivity also corresponds to the variation of lithology. The thickness of superficial fine sand and clay layer increases to SW from 0 m in center to 5-7 m along the Arles-Fos canal. On the other hand, water level decreases to SW from 2-3 m in the NE of marsh area to 0.3-0.7 m SW of marsh. Therefore the thickness of high conductive (low resistivity) superficial layer also increases to SW due to: i) influence of clay content and ii) increase of dissolved salt due to evaporation.

5. Conclusion

Geophysical methods are very useful techniques to inform on the hydrogeological characteristics and calibrate models. Inversed 2D and 3D geophysical models provide high resolution datasets of subsurface structure at a low cost and in a short time. However, this technique still faces difficulty while different resistivity models may produce the same apparent geophysical effect. Therefore, to reduce the errors and

uncertainties in geoelectrical models, it is necessary to compare these models with geological and hydrogeological data.

In the study area, the saltwater front is located around the marsh area where it is distributed in a dense network of ponds, canals and the bulls grazing fields of the bull husbandry industry. Because space for geophysical measurements is very constrained, electromagnetic methods appear useful and need little measurement space. An electromagnetic method using a EM34 device have been applied for mapping the saltwater intrusion with a total investigation length of more than 30km. This method is very simple and rapidly operated at a low cost and on a restrained surface. In order to reduce the errors and uncertainties and to validate results of EM method, a combination of difference geophysics techniques is strongly recommended. Electrical Resistivity Tomography (ERT) was the second choice and developed within this study in three profiles. The advantage of the ERT method is the quality of the electrical resistivity data obtained with relatively high spatial resolution. Both the EM and ERT can be coupled to obtain a continuous coverage of the underground in 2D and 3D spaces. The EM34 data have been interpreted using the software EM4Soil and ERT resistivity interpretation have been done with RES2DINV.

Based on the apparent resistivity/conductivity values obtained from ERT and EM investigations, 3D saltwater distribution was characterized. The low resistivity area is located in the southwest of the study area. Low resistivities were found from 4-5 m.asl close the southwest boundary to more than 20 m.asl near X34, X35 (about 1.7km from the boundary). Observations of water in wells and boreholes also indicate brackish water. In marsh area, low resistivity was found near the surface confirming the presence of a top clay layer and the salinity of surface water caused by evaporation. Outside this area no indication of saltwater or saltwater intrusion has been found.

Based on ERT results, porosity of the aquifer was estimated using the Archie's law for each layers of the aquifer. Data provide detailed information on geometry of the aquifer that can be further interpreted using the lithological descriptions from boreholes.

ACKNOWLEDGEMENTS

This work has been supported by the Project 322 of Ministry of Training and Education (Vietnam) and France government (French-Vietnamese cooperation).

Tài liệu tham khảo

Archie, G. E. (1942, December 1). The Electrical Resistivity Log as an Aid in Determining Some Reservoir Characteristics. Society of Petroleum Engineers. doi:10.2118/942054-G

Borne, V. 1990. La méthode électromagnétique EM 34-3 pour la prospection de sub-surface. Bulletin of the International Association of Engineering Geology - Bulletin de l'Association Internationale de Géologie de l'Ingénieur, 42, 11-20.

BRGM 1995. MARTCRAU: Actualisation du modèle de la nappe de la Crau. 94-D-211, 73.

EMTOMO 2015. EM4Soil-v2.03 – a program for 1D Laterally Constrained Inversion. In: EMTOMO (ed.).

Fitterman, D. V. & Deszcz-Pan, M. 2004. Characterization of saltwater intrusion in South Florida using electromagnetic geophysical methods. 18 SWIM. Cartagena 2004, Spain.

Frohlich, R. K., Urish, D. W., Fuller, J. & O'Reilly, M. 1994. Use of geoelectrical methods in groundwater pollution surveys in a coastal environment. Journal of Applied Geophysics, 32, 139-154.

Goldman, M., Gilad, D., Ronen, A. & Melloul, A. 1991. Mapping of Seawater Intrusion into the Coastal Aquifer of Israel by the Time Domain Electromagnetic Method. Geoexploration, 28, 153-174.

McNeill, J. D. 1980. Electromagnitic terrain conductivity measurement at low conduction numbers. Geonics.

Nguyen Bach Thao, 2016. Coupling geophysical and Isotopic approaches to better simulate saltwater intrusion into coastal aquifers: A case study in the Crau aquifer. *PhD thesis*. University of Avignon, France.

Olioso, A., Lecerf, R., Baillieux, A., Chanzy, A., Ruget, F., Banton, O., Lecharpentier, P., Trolard, F. & Cognard-Plancq, A.-L. 2013. ModellingModeling of Drainage and Hay Production over the Crau Aquifer for Analysing Impact of Global Change on Aquifer Recharge. Procedia Environmental Sciences, 19, 691-700.

Santos, F. A. M., Triantafilis, J., Taylor, R. S., Holladay, S. & Bruzgulis, K. E. 2010. Inversion of Conductivity Profiles from EM Using Full Solution and a 1-D Laterally Constrained Algorithm. Journal of Environmental and Engineering Geophysics, 15, 163-174.

Santos, F. A. M., Almeida, E. P., Castro, R., Nolasco, R. & Mendes-Victor, L. 2002. A hydrogeological investigation using EM34 and SP surveys. Earth Planets and Space, 54, 655-662.

Santos, F. A. M. 2004. 1-D laterally constrained inversion of EM34 profiling data. Journal of Applied Geophysics, 56, 123-134.

Stewart, M. T. 1982. Evaluation of Electromagnetic Methods for Rapid Mapping of Salt-Water Interfaces in Coastal Aquifers. Ground Water, 20, 538-545.
Sasaki, Y. 2001. Full 3-D inversion of electromagnetic data on PC. Journal of Applied Geophysics, 46, 45-54.
SAFEGE 2006. Evolution de la salinité dans le secteur de la Pissarotte. Report 7/2006.
Triantafilis, J., Terhune, C. H. & Santos, F. A. M. 2013. An inversion approach to generate electromagnetic conductivity images from signal data. Environmental ModellingModeling & Software, 43, 88-95.
Triantafilis, J. & Monteiro Santos, F. A. 2013. Electromagnetic conductivity imaging (EMCI) of soil using a DUALEM-421 and inversion modellingmodeling software (EM4Soil). Geoderma, 211–212, 28-38.